Nano Communication Networks 5 (2014) 72–82

Contents lists available at ScienceDirect

Nano Communication Networks

journal homepage: www.elsevier.com/locate/nanocomnet

Capacity and throughput analysis of nanoscale machine communication through transparency windows in the terahertz band

Pavel Boronin [a,b], Vitaly Petrov [a,c], Dmitri Moltchanov [a,*], Yevgeni Koucheryavy [a], Josep Miquel Jornet [d]

[a] Nano Communication Center, Department of Electronics and Communications Engineering, Tampere University of Technology, Tampere, Finland

[b] Communication Networks, St.Petersburg State University of Telecommunications, St.Petersburg, Russia

[c] Broadband Wireless Networking Laboratory, School of Electrical and Computer Engineering, Georgia Institute of Technology, Atlanta, GA, USA

[d] Department of Electrical Engineering, University at Buffalo, The State University of New York, Buffalo, NY, USA

ARTICLE INFO

Article history:
Received 29 May 2014
Accepted 7 June 2014
Available online 20 June 2014

Keywords:
Terahertz band
Ultra-broadband communications
Terabit-per-second (Tbps) links
Graphene

ABSTRACT

The expectedly very limited communication distance of nanoscale machines in the Terahertz Band (0.1–10 THz) is one of the main factors narrowing the scope of the nanonetworking applications. In this paper, the use of the transparency windows in the THz Band, which provide molecular-absorption-free transmission, is proposed as a way to extend the communication distance of nanomachines. The trade-offs between the signal-to-noise (SNR) ratio, channel capacity, transmission bandwidth and communication distance for these windows are identified. The results suggest that, by focusing on the first transparency window (0.1–0.54 THz), reliable communication up to 10 m is feasible when using just 0.1 aJ per symbol to achieve a capacity of up to 10 Mbps. For the same energy per symbol, when using the entire THz Band, the capacity is up to 2 Tbps, but only for distances below a few centimeters. Motivated by these results, the achievable link throughput of a simple binary digital modulation scheme based on the transmission of width-adaptive pulses is investigated. The results show that, due to the relaxation time of molecular absorption noise, additional pauses between pulse transmissions are required, but reliable communication is possible even for very small SNR values. These results extend the application scope of nanonetworks and illustrate that they are not limited to small coverage areas but can also be used to carry traffic generated by both low-rate transactional and bandwidth-greedy applications at small-to-medium distances.

1. Introduction

Nanotechnology is a fast growing research area aimed at, among many others, the development of extremely small machines capable of performing one of few simple actions. Nanotechnology is nowadays considered an enabling technology for a set of applications in biomedical, environmental, and military fields. Being inherently simple and performing primitive operations only, nanomachines in isolation are not expected to manage advanced tasks. To enable more complex applications such as intra-body drug delivery or cooperative environment sensing, the

* Corresponding author.
E-mail addresses: pavel.boronin@tut.fi (P. Boronin), vit.petrov@tut.fi (V. Petrov), dmitri.moltchanov@tut.fi (D. Moltchanov), yk@cs.tut.fi (Y. Koucheryavy), jmjornet@buffalo.edu (J.M. Jornet).

http://dx.doi.org/10.1016/j.nancom.2014.06.001
1878-7789/

exchange of information and commands between networking entities and/or external controller is required. The need for coordination and information sharing naturally leads towards the concept of nanonetworks. One promising way to enable networking capabilities is to use wireless communications between nanomachines [1].

There are several techniques proposed for nanomachine communications including the adaptation of biologically-inspired approaches (e.g., molecular, bacterial, neuronal communications) as well as ultra-high-frequency electromagnetic (EM) communications. Within this list, the latter is one of the most promising techniques. The research on EM nanonetworks started few years ago in the context of nanosensor networks [1]. The early studies concentrated on exploring theoretical basis of communications using miniature transceivers and antennas, understanding the set of frequencies nanomachines can use for communication and analyzing channel characteristics. These early investigations have led to the following findings:

- Graphene can be utilized to develop novel nano-transceivers [2,3] and nano-antennas [4,5], which can efficiently operate in the Terahertz Band (0.1–10 THz) while satisfying the size constraints of nanomachines.
- The THz Band channel is highly frequency selective and exhibits a unique distance-dependent bandwidth behavior due to the absorption mainly from water vapor molecules [6]. In particular, the THz Band behaves as a single transmission window almost 10 THz wide for distances much below one meter, and as a set of multiple-GHz wide windows for longer distances.
- Ultra-broadband communication schemes based on the transmission of ultra-short pulses are an effective way to exploit the very large bandwidth of the THz Band channel for distances much below one meter [7]. The reception of such pulses can be achieved with a simple energy detector [8].
- Nanomachines will require novel energy-harvesting systems to overcome the limitations of their nano-batteries [9,10], which will also change the way in which the protocol stack should be designed [11,12].

For the time being, the focus on EM nanonetworking research has been on increasing the capacity and achievable data rates when utilizing ultra-broadband signals that occupy the entire THz Band. For example, in [6], under realistic energy constraints, it is shown that Terabit-per-second (Tbps) links are possible among nanomachines, but only for distances much below one meter. However, it is relevant to note that, in many prospective applications of EM nanonetworks, the communication range is more important than the data rate. Examples of such applications include transactional type of networks, e.g., environment monitoring networks or command/response type of networks. Thus, it is important to find a way to increase the coverage of a single node.

In this paper, we first propose a way to mitigate molecular absorption by properly choosing the range of frequencies known as transparency windows. Then, we discuss trade-offs and dependencies between the choice of the window, its bandwidth and capacity, and the communication range of a single node. We show that the smart selection of bandwidth with respect to the level of molecular absorption leads to way better performance of our system in terms of communication range and capacity. In particular, our results indicate that for a nominal power of 26.5 nW (equivalent to a 100 fs-long pulse with 0.1 aJ energy) the communication range can be up to 15 m providing satisfactory capacity for transactional applications in the range of 4–11 Mbps. Such a range is only possible when operating in the lower end of the first transparency window 0.1–0.54 THz. Moving up in the spectrum to the next transparency window, the free-space propagation loss dominates the channel characteristics prohibiting long communication distances. Using the whole window bandwidth one can get up to 2 Tbps at 0.01 m.

Motivated by these results, we investigate the achievable throughput of a simple binary digital modulation built on top of a novel width-adaptive pulse-based communication scheme. We also extend the model presented in [6,7] by incorporating the effect of molecular relaxation. Our results show that, due to the molecular absorption relaxation time, additional pauses between pulse transmissions are required, but reliable communication is possible even for very small signal-to-noise ratio (SNR) values. These results expand the application scope of nanonetworks and illustrate that they are not limited to small coverage areas but can also be used to carry traffic generated by both low-rate transactional and bandwidth-greedy applications at small-to-medium distances. Similar results for macroscale THz Band communication networks have been recently discussed in [13]. As we will discuss in this paper, the distance drastically affects the transparency windows and, thus, our analysis, which is focused on nanoscale machine communication, is novel.

The rest of the paper is organized as follows. In Section 2, we briefly review the THz Band channel characteristics. In Section 3, we identify and discuss the properties of transparency windows in the THz Band and then study trade-offs and dependencies between communication distance, SNR and capacity. The throughput of a width-adaptive pulse-based communication system is analyzed in Section 4 and numerical results are provided in Section 5. Conclusions are drawn in Section 6.

2. Terahertz Band channel characteristics

The link budget equation for the received power in the THz Band can be represented as

$$P_{Rx}(f, d) = P_{Tx}(f) - L_P(f, d) - L_A(f, d), \quad (1)$$

where P_{Tx} is the power spectral density (p.s.d.) of the transmitted signal, P_{Rx} is the p.s.d. of the received signal, L_P is the free-space propagation loss, and L_A is the p.s.d. of the molecular absorption loss. In addition to the two contributions to the path loss, the received signal is also affected by the molecular absorption noise. Note that the thermal noise when using graphene-based nano-antennas and nano-transceivers is currently not known, but expectedly very low [14,15], which implies that noise is mostly due to molecular absorption noise created in response to absorption of EM waves by molecules in the channel.

2.1. Molecular absorption loss

The presence of molecular absorption loss L_A due to internally vibrating molecules is a unique feature of the THz Band. The molecular absorption of EM waves is the effect occurring when the frequency of the wave is close to the resonant frequency for internal vibrational modes of a molecule. Vibrating molecules absorb EM energy and convert it to kinetic energy. The ability of the molecule to absorb energy is determined by their physical properties (bond structure, spatial orientation, etc.) and is measured by the absorption coefficient. Water vapor molecules dominate the absorption in standard medium conditions.

Following [6], the absorption loss is characterized by

$$L_A(f, d) = \frac{1}{\tau(f, d)}, \tag{2}$$

where f is the operating frequency, d is the separation distance between the transmitter and the receiver, while τ is the transmittance of the medium that can be well approximated by the Beer–Lambert law

$$\tau(f, d) = e^{-K(f)d} = e^{-\sum_{G,I} K_{G,I}(f)d}, \tag{3}$$

where K is overall absorption coefficient which is estimated by summing up individual absorption coefficients, $k_{G,I}$, of molecules of a single isotopologue I of gas G. The latter is determined as

$$k_{G,I}(f) = \frac{p}{p_0}\frac{T_0}{T} Q_{G,I}\sigma_{G,I}(f), \tag{4}$$

where p and T are the pressure and temperature of the medium, p_0 and T_0 are the standard pressure and temperature, respectively, $Q_{G,I}$ is the volume density of molecules measured in molecules/m^3, and $\sigma_{G,I}$ is the cross-section absorption measured in m^2/molecule. The latter two parameters are given by

$$Q_{G,I} = \frac{pL}{RT} Q_{G,i}, \qquad \sigma_{G,I}(f) = S_{G,I} G_{G,I}(f), \tag{5}$$

where R is the gas constant (8.31 J/K tmol), L is the Avogadro constant (the number of molecules per mole, $6.02 \cdot 10^{23}$ mol^{-1}), $S_{G,I}$ is the linear absorption intensity, and $G_{G,I}$ is the form of the spectral component. Both $S_{G,I}$ and $G_{G,I}$ are tabulated in [16] and analytically estimated in [6]. Some additional corrections to $G_{G,I}$ are needed when special conditions (pressure/temperature) are considered. In this case, one needs to first determine the resonant frequency of each isotopologue I. It is important to note that the increase in pressure results in the linear increase of the resonant frequency implying that the absorption increases as well. However, for common pressure variations, the resulting change in L_A is almost non-existent.

The absorption coefficient, K in (3), for $T = 296$ K and 1.8% concentration of water vapor for 0.1–5 THz is shown in Fig. 1. This has been obtained by utilizing the procedure in [6] with the information contained in the HITRAN database [16]. One important observation is that the molecular absorption is a highly frequency selective process. At some frequencies, the absorption is very high and may eventually result in an extremely small communication range. However, we see that at the so-called transparency windows, the absorption is significantly smaller than in the rest of the band. Note that K is independent of d; however, the absorption loss, L_A, does depend on the distance, via (2) and (3). Thus, in order to provide the longest possible communication range, K must be at minimum.

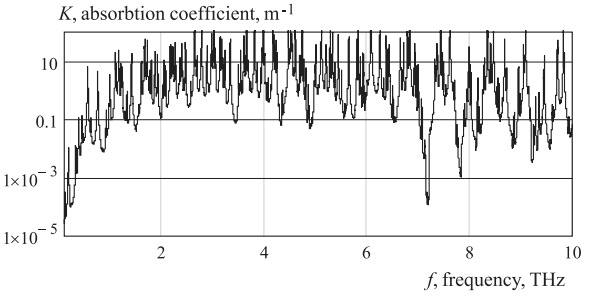

Fig. 1. The absorption coefficient K [16].

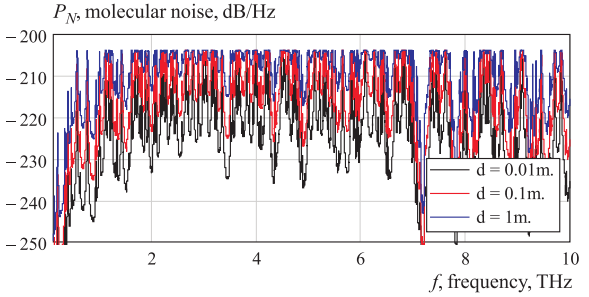

Fig. 2. The molecular absorption noise p.s.d.

2.2. Molecular absorption noise

Molecules convert part of the absorbed energy into kinetic energy. At the same time, part of this energy is reemitted in the channel, effectively creating the so-called molecular absorption noise. The p.s.d. P_N of molecular absorption noise is given by [6]

$$P_N(f, d) = k_B[N_M(f, d) + N_A(f)], \tag{6}$$

where k_B is the Boltzmann constant and N_M is the equivalent molecular absorption noise temperature, given by

$$N_M(f, d) = T\varepsilon(f, d) = T[1 - \tau(f, d)], \tag{7}$$

where ε stands for the emissivity of the medium, and N_A is the temperature of other noise sources at frequency f. Traditionally, the most important component of N_A is the electronic thermal noise at the receiver. For the time being, to the best of our knowledge, an accurate noise model for graphene-based devices does exist, but it is expectedly very low and will not be considered in our analysis [15].

In Fig. 2, the p.s.d. of molecular absorption noise, given by (6), is illustrated for $d = 0.01, 0.1, 1$ m, $T = 296$ K and 1.8% concentration of water vapor. The situation is qualitatively similar to Fig. 1 in the sense that in some frequency ranges the molecular absorption noise is significantly lower than in the others. When the transmittance of the medium is less than 94.5% the molecular absorption

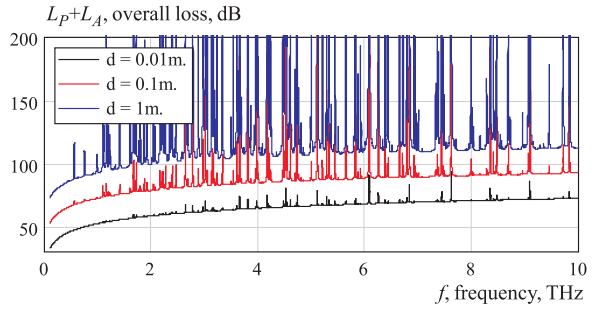

Fig. 3. The total path loss (molecular absorption loss and free-space propagation loss).

noise p.s.d. increases from 100 to 10,000 times having the maximum value at −204 dB/Hz. While this value seems to be low, when integrated over a very large channel bandwidth, it can result into very high noise powers.

Note that when the transmittance is below 5.5%, the molecular absorption noise is relatively big. The corresponding molecular absorption is in-between 0 and 0.25 dB. This implies that the transmitted signal is mostly affected by absorption noise rather than attenuated by absorption loss (e.g., 30 dB of noise compared to 0.25 dB of absorption).

2.3. Free-space propagation loss

Free-space propagation loss is another parameter heavily affecting the received signal power. In fact, as will be shown further, for a certain set of frequencies in the THz Band, the absorption loss is a dominating factor determining the achievable range of communications.

The free-space propagation loss can be described as

$$L_P(f, d) = \left(\frac{4\pi f d}{c_0}\right)^2, \tag{8}$$

where c_0 is the speed-of-light in the medium of interest (for open air $c_0 \approx 3 \cdot 10^8$ m/s), d is the separation distance between the transmitter and the receiver, and f is the frequency of interest. As one may observe, the increase of the frequency results in the quadratic increase of the free-space propagation loss. When transparency windows are considered, the free-space propagation loss becomes the dominating factor limiting the coverage area of the transmitter. This also implies that, in order to extend the communication range, one should use transparency windows with lower frequencies.

Fig. 3 shows the overall loss (molecular absorption and free-space propagation loss) for $d = 0.1, 0.01, 1$ m distances, $T = 296$ K, 1.8% of vapor, in the 0.1–5 THz Band. We see that at most frequencies the dominating loss factor is molecular absorption. However, in the transparency windows the molecular absorption is almost non-existent.

3. Communication in transparency windows

In spite of quite complex channel characteristics, there is a way to avoid severe signal distortion by using the *transparency windows*. In these windows, the transmittance of the medium, $\tau(f, d)$ in (3), is never smaller than 95% for a certain d. This implies that, in these transparency windows both the molecular absorption loss and noise level are as small as feasible. In this section, we will first demonstrate and discuss the propagation characteristics of transparency windows in the THz Band. Then, we will study the trade-offs between channel capacity, available bandwidth, transmission power and communication range of a single nanomachine.

3.1. Channel characteristics of transparency windows

There are many transparency windows available in the THz Band. However, the property of accumulating the molecular absorption loss and noise with the distance does not allow us to precisely determine the transparency windows as they are dependent on the distance. In this paper, the choice of these windows is performed based on the transmittance τ (3) as discussed above. Otherwise the p.s.d. of molecular absorption noise takes on its maximal value of −203.89 dB/Hz (e.g., for the 50 GHz channel the maximal value will be −97 dB). We consider only those windows with at least 50 GHz of bandwidth.

Table 1 summarizes the properties of the transparency windows available in the 0.1–10 THz frequency range. The number of these windows decreases with the distance d. For example, at 0.01 m distance, there are more than 15 of these windows in the THz Band and the first three are 0.1–0.54 THz ($B = 440$ GHz), 0.57–0.72 THz ($B = 150$ GHz) and 0.78–0.93 THz ($B = 190$ GHz). At 1 m distance there are only six windows left and these are the windows represented in Table 1. These first three windows are the only possibility for extending the communication range as other three available windows are located in the upper part of the THz Band, where the level of free-space loss drastically impacts the communication over distances greater than several millimeters. When going from 0.01 m to 1 m, the bandwidth of the third window drastically decreases, while the first and second windows remain almost intact. The column referring to equivalent pulse duration will be discussed later, to analyze the throughput of width-adaptive pulse-based communications.

To illustrate the gain of using the first transparency window, the term $1/L_P L_A N_m$ is shown at a function of frequency in Fig. 4 for $d = 0.01, 0.1, 1$ m, $T = 296$ K and 1.8% concentration of water vapor. As one may observe, using the whole first transparency window, communication distances of up to several centimeters might be achievable. In what follows, we will explore this possibility in more detail.

3.2. Signal-to-noise ratio versus distance

Independently of the modulation, one of the major factors affecting the achievable data rate is the SNR. In Fig. 5, the SNR is illustrated as a function of distance for five channels in the first transparency window, 0.1–0.15 THz and 0.1–0.2 THz (50 GHz and 100 GHz sub-bands in the beginning of the window), 0.44–0.54 and 0.49–0.54 THz (50 GHz and 100 GHz sub-bands in the tail of the window) and the whole window's bandwidth 440 GHz assuming that the

Table 1
Transparency windows at different distances.

Number	Dist. (m)	Freq. (THz)	Width (GHz)	Pulse (ps)
	0.01	0.10–0.56	457	1.36
1	0.1	0.10–0.55	445	1.40
	1	0.10–0.54	440	1.48
	0.01	0.56–0.75	192	3.23
2	0.1	0.57–0.74	173	3.59
	1	0.63–0.72	95	6.53
	0.01	0.75–0.99	237	2.62
3	0.1	0.76–0.98	218	2.85
	1	0.76–0.98	126	4.92
	0.01	7.00–7.33	330	1.88
4	0.1	7.01–7.31	300	2.07
	1	7.07–7.23	160	2.59
	0.01	7.64–7.98	340	1.83
5	0.1	7.72–7.96	240	2.59
	1	7.75–7.88	130	3.88
	0.01	8.01–8.28	270	2.30
6	0.1	8.04–8.15	110	5.64
	1	8.04–8.15	80	7.76

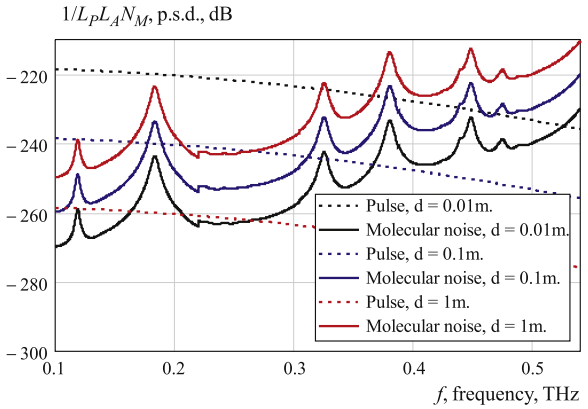

Fig. 4. $1/L_PL_AN_M$ for different distances d.

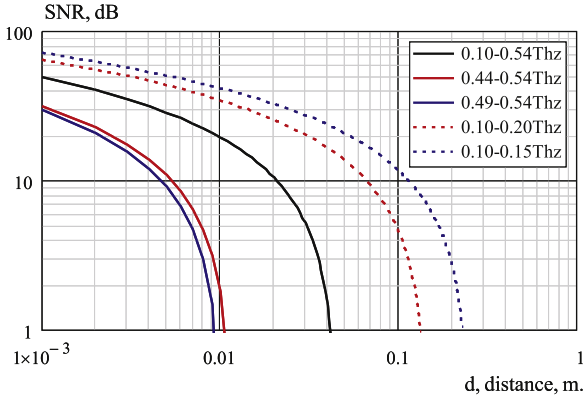

Fig. 5. SNR for selected bandwidths in the first window.

water filling is used with a total power to distribute equal to 26.5 nW. First of all, we see that communication ranges of few centimeters can be achieved operating in the first transparency window. When the whole window is used the SNR drops below 10 dB at approximately 0.02 m. Further, we see that there is a significant difference between

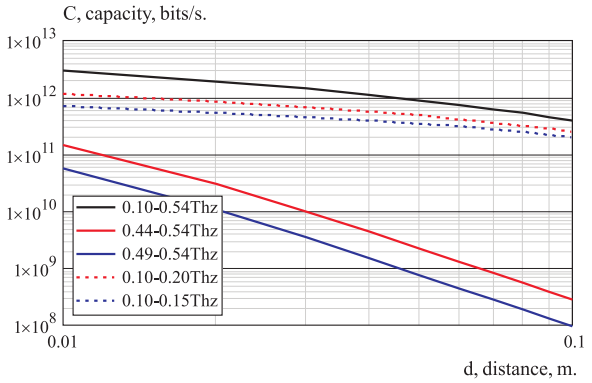

Fig. 6. Capacity for selected bandwidths in the first window.

channels in the beginning of the window and at the end of it. The reason is that the dominating effect of the free-space propagation loss as the absorption loss and molecular absorption noise provide rather limited contribution to the SNR. In particular, using the 50 GHz channel in the beginning of the band one could reach distances of up to 0.1 m while keeping the SNR higher than 10 dB and using extremely small energy. These results implies that one could enable nanomachines communicating over significantly larger distances enabling networking with micro- and macro-devices.

3.3. Capacity versus distance

Under the common assumption that the transmitted signal and the total noise are jointly Gaussian, the capacity C of the transparency windows is estimated by using the classic Shannon result

$$C(d) = \int_{B(d)} \log_2 \left(1 + \frac{P(f)}{L_P(f,d)L_A(f,d)N_M(f,d)}\right) df, \quad (9)$$

where B is the distance-dependent channel bandwidth, P is the transmitted signal p.s.d., L_P is the free-space propagation loss, and N_M is the molecular absorption noise p.s.d. Since we are concerned only with transparency windows the effect of the absorption loss L_A is negligible. Further, the effect of thermal noise is also close to non-existent. In all calculations, a standard environment has been assumed ($T = 296$ K, $p = 760$ mmHg, 1.8% of vapor molecules).

In Fig. 6, the channel capacity is shown as a function of distance (in log–log scales) for five channels in the first transparency window, 0.1–0.15 THz and 0.1–0.2 THz (50 GHz and 100 GHz sub-bands in the beginning of the window), 0.44–0.54 and 0.49–0.54 THz (50 GHz and 100 GHz sub-bands in the tail of the window) and the whole window bandwidth 440 GHz assuming 26.5 nW of total power. Recalling SNR results where SNR values for the "best" 50 GHz channel in the beginning of the window drops below 10 dB around $d = 0.1$ m, we limit the maximum distance to 0.1 m. First of all, notice that using the whole window bandwidth of 440 GHz one can get extremely high capacity of few Tbps at relatively small distances of up to few cm (around 2 Tbps at 0.01 m). The latter is significantly better coverage compared to

few millimeters reported in [6] for the whole 0.1–10 THz range. The capacity of the channel is comparable to that one obtained in [6] for the whole range (0.7–2 Tbps vs. 1–5 Tbps). At the distance 0.02 m corresponding to an SNR of 10 dB using the whole windows one obtains approximately 0.7 Tbps.

Decreasing the channel bandwidth while using the total power, larger distances are achievable at the expense of smaller capacity. Recalling Fig. 5, the most efficient way would be to use the channels in the beginning of the window. Indeed, observing Fig. 6, we see that keeping the channel bandwidth intact while moving them to the tail of the window decreases the achievable distance by more than 10 times. The same trend is observed for channel capacity. First of all, as expected, 100 GHz channels outperform 50 GHz sub-bands in both cases. Further, both sub-bands in the beginning of the window outperform their counterparts in the tail of the window. The difference becomes bigger with the distance and could be as large as several orders of magnitude. This effect is again due to propagation loss with molecular absorption noise providing insignificant impact. In absolute numbers all the considered channels provide more than sufficient capacity for transactional type of applications. The whole window of 440 GHz width as well as 50 GHz and 100 GHz channels in the beginning of the window can also be used for extremely rate demanding applications at distances of up to few centimeters, e.g., exchange of data between cores in multi-core processors or other computational components.

3.4. Trading-off capacity for distance

Discussing the results provided in Figs. 7 and 8, we observed that decreasing the bandwidth of the channels, while keeping the total power constant, leads to extended coverage. The side effect is however the reduced channel capacity. Here we will explore this trade-off in detail showing that a very large communication range can be achieved. With such a trade-off we explicitly target transactional type of applications for which the requirements for capacity are not that high but the separation distance could be substantial. This is especially important for nano- and micro-world applications, where resource-constrained end systems will not need to handle the information at high rates anyway. Also, the larger communication range is of higher importance in many applications of this type.

The SNR for 1, 10, 100 and 1000 MHz channels chosen in the beginning of the window starting from 0.1 THz is shown in Fig. 5. Using 10 dB as the lower limit we see that distances from one up to few meters are reachable. The corresponding capacities are illustrated in Fig. 8. Note that the channel capacity is still sufficient for transactional type of applications exchanging small amounts of data between each other or with a gateway, e.g., environmental state observations like temperature, air condition, etc. In particular, for the 1 MHz channel one gets from 11 to 4 Mbps in the range 0.1–10 m, while for the 1 GHz channel from 11 to 4 Gbps in-between 0.1–1 m. Recalling that the whole windows's bandwidth provides the rate of up to 2 Tbps for relatively small distance (up to 0.02 m) we see that working in the first window one may target applications with completely different rate and communication range requirements.

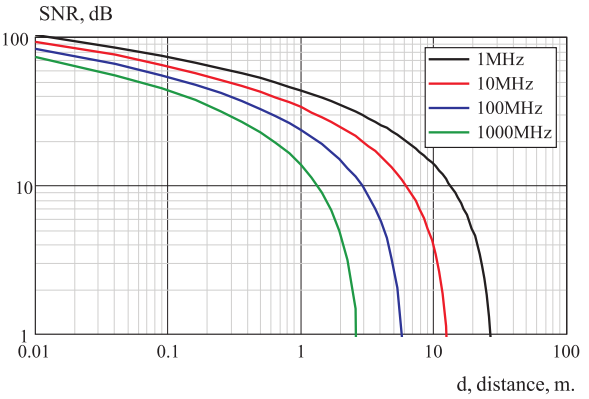

Fig. 7. SNR for selected bandwidths near 0.1 THz.

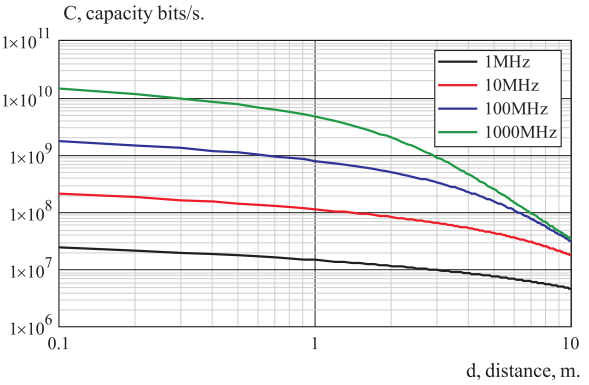

Fig. 8. Channel capacity for selected bandwidths near 0.1 THz.

4. Achievable throughput and bit error rate

In this section we analyze the link throughout and the Bit Error Rate (BER) of a simple pulse-based modulation scheme for communication in the transparency windows.

4.1. Width-adaptive pulse-based On–Off Keying

The capacity analysis in the previous section provides us an upper bound on throughput at a certain distance d. In practice, the actual throughput of the channel also depends on the chosen Modulation and Coding Scheme (MSC). Due to performance and energy constrains for prospective devices only extremely simple MSC could be applied to nanonetworks.

In this paper we focus on a simple On–Off Keying modulation scheme built on top of a pulse-based communication mechanism (see Fig. 9). In particular, the transmitter uses a wide-band pulse of a certain duration Δt to represent a logical 1 and keeps silent for the same amount of time to represent a logical 0. The pulse duration Δt depends on the channel bandwidth B, which on its turn depends on the transmission distance d (see Table 1). There is also a

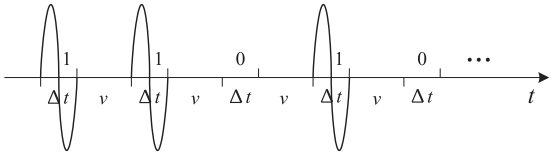

Fig. 9. An illustration of pulse-based On–Off Keying.

guard interval between symbols of duration v that depends on the operating frequency f (a particular choice of the sub-band in the THz Band) and may also depend on the distance from the transmitter as discussed below. Such a scheme allows us to use simple energy detectors in reception [8].

For this modulation, the raw throughput T_R is given by

$$T_R(B, f, d) = \frac{1}{\Delta t(B) + v(f, d)}. \tag{10}$$

In what follows, we will concentrate on the channel spanning the whole bandwidth of the first transparency window, 0.1–0.54 THz. Due to this reason we will drop dependence of B and f and use Δt and $v(d)$ to denote the pulse duration and inter-symbol interval, respectively.

4.2. The impact of molecular absorption relaxation

We analyze next the impact of molecular absorption on the transmission of pulses. When a simple energy detector is used as a receiver, v can be made infinitesimally small for relatively high SNR values (e.g., more than 10 dB) by choosing a sufficiently small energy detection threshold P_T. However, even when the signal amplitude gets smaller and comparable to the noise, we can still correctly receive transmitted symbols. The reason is that the molecular absorption noise gradually decrease after the pulse transmission. That is, as long as we choose a proper value of the inter-symbol interval v and proper energy detection threshold P_T, we may still successfully receive the information even when the SNR is small. Although under these conditions it becomes difficult to distinguish signal from the noise, we may still decide upon reception of 1 or 0 based on the mixture of signal and noise. Performing this "noise-assisted" reception we may extend the communication range of nanomachines even further and keep non-zero throughput at distances characterized by a low SNR. We also expect that in this low-SNR regime the optimal value of the energy detection threshold may also depend on the distance.

In order to detect the mixture of noise and signal when the SNR is low we have to allow for some time period between pulses for molecular relaxation, v. The molecular absorption noise relaxation time T_R is defined as the amount of time required for excited molecules to reduce their amplitudes below 10%. According to [17,18], the relaxation time T_R is at least 1 ps. Note that the precise data for our conditions does not seems to be available. In general, the relaxation time is a complex function of many parameters and depends on the state of matter (increases as we go from ice to liquid to vapor). In the vapor state, it decreases with temperature as higher temperature causes additional excitation adding to the background noise in the channel. Thus, we will take 1 ps as a lower bound of the relaxation time. We model the process of molecular relaxation using exponentially decaying function in the form

$$R(f, t, d) = R_{f,A}(d)e^{-\gamma t}, \tag{11}$$

where $R_{f,A}$ is the noise amplitude at the end of pulse transmission (we will consider this time instant as $t = 0$) at the distance d, and γ is the rate of molecular relaxation that can be estimated using the molecular relaxation time T_R ($\gamma \approx 2.303$ for $T_R = 1$ ps and $\gamma \approx 0.461$ for $T_R = 5$ ps).

4.3. Received signal time-domain representation

To illustrate the effect of noise on the attenuated pulse we approximate the noise structure in the time domain. It is important to note that the form of the noise in the time domain could hardly be recovered exactly due to the absence of the phase spectrum. The task is then to find time-domain representation of noise having a given power spectrum. There are several techniques that can be applied to obtain the approximated form of the noise, e.g., Hermitian signal processing, conjugate approach, etc.; see [19, pp. 11–13]. All these approaches are technically based on the complex baseband inverse fast Fourier transform (IFFT).

To obtain time-domain representation of the noise at a certain distance, we first sample the noise power spectral density with high frequency $B = f_{i+1} - f_i$. The noise component between f_i and f_{i+1} is approximately frequency-flat and can be approximated by a cosine function with amplitude A_i proportional to $\sqrt{2N_iB}$. Further, observing that the noise in transparency windows is characterized by very low correlation between components on different frequencies we represent components of the phase spectrum ϕ_i using the uniform distribution between 0 and 2Π. The resulting approximation of the noise in the time domain is given by

$$N(t) = \sum_{n=1}^{N} A_n \cos(2\pi f_n t + \phi_n), \tag{12}$$

where N is the number of samples.

Having the form of the noise and pulse in the time domain we can illustrate the noise effect on a particular pulse shape. Fig. 10 shows a random realization of the noise N, the attenuated pulse S and the received pattern $[S(t, d)+N(t, d)]R(f, t, d)$ at different distances d from the transmitter, where R is the process of molecular relaxation; see (11). In these illustrations we use the Gauss-shaped pulse (half of the pulse is shown). However, in order to put the power of the pulse into 0.1–0.54 THz transparency window we will use a monocycle, a first derivative of the Gaussian-shaped pulse. As one may observe the pulse gets completely distorted by molecular noise at distances larger than 0.06–0.07 m (the SNR is less than 1) and is almost distorted when transmitted over 0.05 m (the SNR is around 1; SNR values are presented in Fig. 5). Similar methodology could be used to illustrate distortion of more complicated pulses.

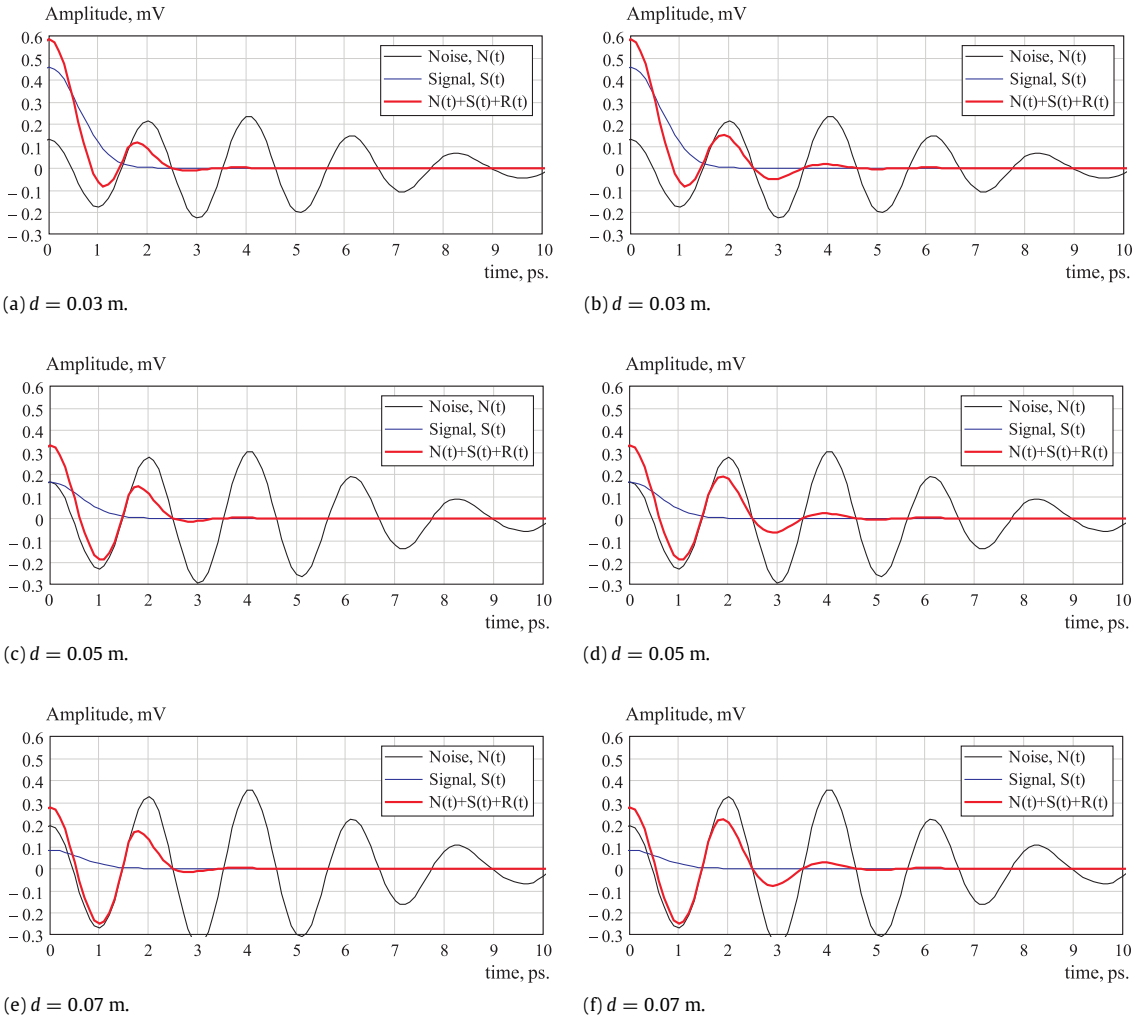

(a) $d = 0.03$ m. (b) $d = 0.03$ m.

(c) $d = 0.05$ m. (d) $d = 0.05$ m.

(e) $d = 0.07$ m. (f) $d = 0.07$ m.

Fig. 10. Example of time-domain behavior of the received signal.

4.4. Error probability

In order to obtain the bit error rate we consider a simple energy detector (described in detail in [8]) as a receiver. According to the energy detector, we get 1 as long as the amount of the power received in Δt is greater than a certain power threshold P_T.

Consider the bit stream at the input to the binary On–Off encoder and assume that no channel coding is performed. Observing transmissions of 1 and 0 in isolation we see that the energy detection threshold provides no effect when 0 is transmitted. In other words, P_T could be chosen arbitrarily small (still higher than the background noise which is neglected in this study). On the other hand when 1 is transmitted P_T should be chosen such that the probability that the received sum of power and noise is greater than P_T is maximized. Working in time domain the probability of incorrect reception of one is given by

$$p_{1,E}(d) = \Pr\left\{\int_0^{\Delta t} [S(t,d) + N(t,d)]^2 dt < P_T(d)\right\}. \quad (13)$$

When the transmission of 0 and 1 is considered in isolation (13) dictates to use the smallest possible value of P_T that is still higher than the background noise. In practice, the molecular absorption noise generated in response to the presence of energy (pulse) in the channel prohibits us from using extremely small values of P_T. To demonstrate it consider different tuples of binary input to the channel. We see that molecular absorption noise provides no negative effect when tuples 11, 01 and 00 are transmitted. However, when tuple 10 is transmitted the molecular absorption noise created by the preceding 1 may affect the decision made for 0. The conditional probability of incorrect reception of 0 in a sequence 10 is then

$$p_{10,E}(v, P_T, d) = \Pr\left\{\int_{v(f,d)}^{v(f,d)+\Delta t} [S(t,d) + N(t,d)]R(f,t,d)dt < P_T\right\}, \quad (14)$$

where we assume that the pulse ends at $t = 0$, v is the inter-symbol interval, Δt is the duration of the symbol,

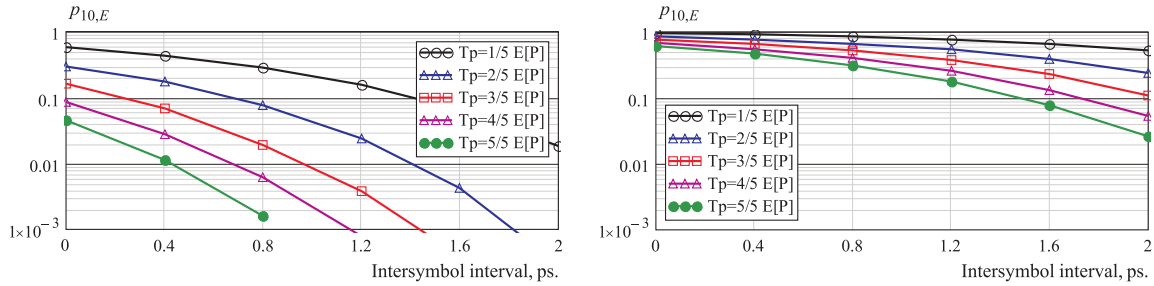

(a) Conditional error probability of 0 in 10 for $d = 0.05$. (b) Conditional error probability of 0 in 10 for $d = 0.07$.

Fig. 11. Probability of incorrect reception of 0 after 1.

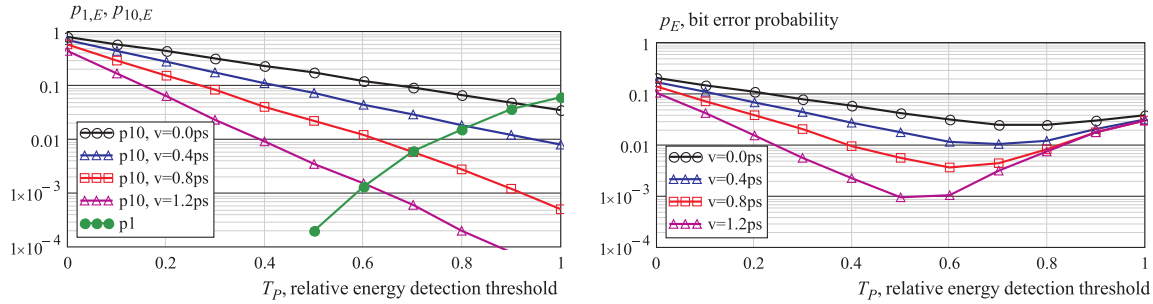

(a) Unconditional and conditional error probabilities. (b) Bit error probability, p_E.

Fig. 12. $p_{1,E}$, $p_{10,E}$, p_E as a function of v, P_T for $d = 0.05$. (For interpretation of the references to color in this figure legend, the reader is referred to the web version of this article.)

$R(f, t, d)$ is the molecular relaxation, $S(t, d)$ and $N(t, d)$ are the pulse and noise at the distance d from the transmitter, respectively. In what follows we investigate behavior of these two metrics.

5. Numerical results

We perform numerical analysis of throughout and associated BER using the simulation study. The major point of the study is the trade-off between correct reception of 1 ($p_{1,E}$) and 0 (in the sequence 10, $p_{10,E}$) caused by different values of power detection threshold P_T and inter-symbol time τ. Further, we are mainly interested in those regions where the SNR is below than few decibels. In our analysis we are mostly concentrated in qualitative results for low values of SNR.

5.1. Bit error rate

Fig. 11 shows $p_{10,E}$ for $d = 0.05$ m (SNR $\approx$ 1 dB) and $d = 0.07$ m (SNR $<$ 1 dB) for relaxation time $T_R = 5$ ps as a function of inter-symbol time interval v and power detection threshold T_P. It is important to note that the values of T_P were chosen with respect to the mean attenuated signal power at a certain distance, $E[P] = \int_0^{\Delta t} S^2(t, d)dt$ starting from $E[P]/5$ up to $E[P]$ with a step size of $E[P]/5$. As one may observe, the probability of incorrect reception of 0 after 1 decreases as a function of both inter-symbol interval τ and power detection threshold T_P. As we expected the decrease of $p_{10,E}$ is exponential in response to the increase v while the corresponding decrease in throughput is linear. The effect of P_T is also positive. As an example, for $v = 0.8$ ps changing the value of T_P from $E[P]/5$ to $E[P]$ results three orders of magnitude decrease in $p_{10,E}$. However, the latter effect cannot be considered in isolation neglecting the probability of incorrect reception of 1 as the increase in the energy detection threshold should negatively affect $p_{1,E}$.

Since in a number of applications the nanomachines are supposed to be extremely primitive and implement no complex error correction algorithms, BER could be the most important metric of interest. Fig. 12 shows $p_{10,E}$, $p_{1,E}$ and BER, p_E, for $d = 0.05$ m, $T_R = 5$ ps and for few values of v and P_T. First of all, recall that v does not affect $p_{1,E}$ implying that $p_{1,E}$ is constant for any chosen value of v (green line in Fig. 12(a)). Further, we see that considering BER as the only metric of interest the inter-symbol interval v plays a simple role as the minimum value of BER is obtained by setting v to the biggest possible value and appropriately choosing the energy detection threshold, P_T. Note that the value of P_T optimizing BER for a given v depends on the distance between the transmitter and the receiver. For $d = 0.05$, $v = 1.2$ ps, $T_R = 5$ ps this value is in-between $0.5 \times E[P]$ and $0.6 \times E[P]$.

5.2. Throughput

Recall that the value of the inter-symbol time interval v affects not only the bit error probabilities considered in the previous subsection but the throughput of the system as well. The raw throughput of the system for several values of v ($d = 0.05$ m, $T_R = 5$ ps) is shown in Fig. 13(a). As expected the raw throughput linearly decreases in response to the linear increase in v.

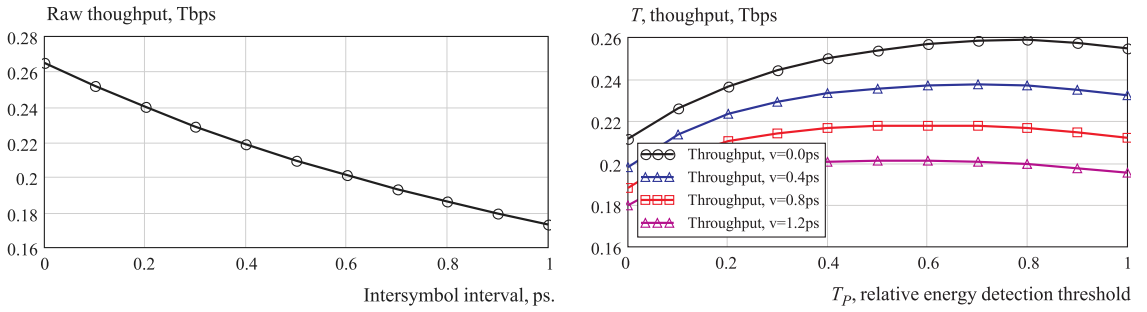

(a) Raw throughput.

(b) Effective throughput.

Fig. 13. System throughput as a function of v for $d = 0.05$.

Fig. 13(b) demonstrates the obtained throughput defined as $T(1 - p_E)$, i.e., the fraction of bits that are correctly received. Observing the data provided in Figs. 12 and 13 altogether there are a number of important observations. First of all, having throughput as an ultimate metric of interest we see that the inter-symbol interval v is independent of d for small values of SNR. In fact, setting $v = 0$ ps provides us with the best possible throughput if the value of the energy detection threshold is set properly. In its turn, the optimal value of P_T does depend on the distance and for $d = 0.05$ m it is approximately $0.8 \times E[P]$. For other values of d the optimal value of P_T changes. From the other hand, one may notice that the difference in throughputs for different values of v is rather small. For example, the maximum difference between inter-symbol intervals $v = 0.0$ ps and $v = 1.2$ ps is attained at $P_T \approx 0.8$ and is approximately 23% (0.06 Tbps).

We note that the results provided here are based on several assumptions and approximations. Although they allowed us to reveal a number of important trade-offs and dependencies, in order to understand the behavior of the optimal values of P_T for different d more complex models of molecular absorption noise in power and time domain are required. On top of this, analytical models can be further used to describe the behavior of the system for a wider range of input parameters.

6. Conclusion

In this paper, we advocated the use of transparency windows in the THz Band to enable communications between nanomachines. When using these windows the communication range of a single node significantly increases as molecular absorption is close to non-existent. In these windows the free-space propagation loss becomes the dominating factor in channel characteristics. As a result, although there are a number of transparency windows in the THz Band the one allowing us to achieve the larger distances is the first one, 0.1–0.54 THz. We demonstrated that using the nominal pulse energy of 0.1 aJ and one channel of 1 MHz width in this window one can achieve the communication range of up to 15 m still providing respectable capacity on the order of 4–11 Mbps. Increasing the bandwidth of the channel in the transparency window the coverage decreases but the capacity increases linearly. Thus, depending on the needs of prospective applications one could make a wise choice of parameters satisfying coverage and capacity constraints.

By analyzing the throughput of the system for a simple On–Off keying modulation built on top a width-adaptive pulse-based scheme we demonstrated that reception is possible even for small values of SNR ($\tilde{1}$ dB) corresponding to large distances (0.05 m for the 0.1–0.54 THz transparency window). Both the inter-symbol time v and power detection threshold P_T affect the bit error rate. Both of these parameters decrease the probability of incorrect reception of 0 after 1 while the latter also affects the unconditional probability of incorrect reception of 1. For a certain distance d there is an optimal point corresponding to the highest achievable system throughput and minimal BER. In order to investigate the behavior of the optimal point in more detail additional studies are needed.

Acknowledgments

This work was supported by the FiDiPro program of Academy of Finland "Nanocommunication Networks", 2012–2016. The authors are also grateful to A. Ozan Bicen (BWN Lab, School of Electrical and Computer Engineering, Georgia Institute of Technology, Atlanta, Georgia, USA) for helpful discussions and insightful comments in the course of this work.

References

[1] I.F. Akyildiz, J.M. Jornet, Electromagnetic wireless nanosensor networks, Nano Commun. Netw. (Elsevier) J. 1 (1) (2010) 2–19.
[2] L. Vicarelli, M.S. Vitiello, D. Coquillat, A. Lombardo, A.C. Ferrari, W. Knap, M. Polini, V. Pellegrini, A. Tredicucci, Graphene field-effect transistors as room-temperature terahertz detectors, Nature Mater. 11 (2012) 865–871.
[3] J.M. Jornet, I.F. Akyildiz, Graphene-based plasmonic nano-transceiver for terahertz band communication, in: Proc. of European Conference on Antennas and Propagation, EuCAP, 2014.
[4] M. Tamagnone, J.S. Gomez-Diaz, J.R. Mosig, J. Perruisseau-Carrier, Reconfigurable terahertz plasmonic antenna concept using a graphene stack, Appl. Phys. Lett. 101 (21) (2012) 214102.
[5] J.M. Jornet, I.F. Akyildiz, Graphene-based plasmonic nano-antenna for terahertz band communication in nanonetworks, IEEE J. Sel. Areas Commun. 12 (12) (2013) 685–694. Special Issue on Emerging Technologies for Communications.
[6] J.M. Jornet, I.F. Akyildiz, Channel modeling and capacity analysis for electromagnetic wireless nanonetworks in the terahertz band, IEEE Trans. Wireless Commun. 10 (10) (2011) 3211–3221.
[7] J.M. Jornet, I.F. Akyildiz, Femtosecond-long pulse-based modulation for terahertz band communication in nanonetworks, IEEE Trans. Comm. 62 (5) (2014) 1742–1754.

[8] R.G. Cid-Fuentes, J.M. Jornet, I.F. Akyildiz, E. Alarcon, A receiver architecture for pulse-based electromagnetic nanonetworks in the terahertz band, in: Proc. of IEEE International Conference on Communications, ICC, June 2012, pp. 4937–4942.
[9] J.M. Jornet, I.F. Akyildiz, Joint energy harvesting and communication analysis for perpetual wireless nanosensor networks in the terahertz band, IEEE Trans. Nanotechnol. 11 (3) (2012) 570–580.
[10] Z.L. Wang, Towards self-powered nanosystems: from nanogenerators to nanopiezotronics, Adv. Funct. Mater. 18 (22) (2008) 3553–3567.
[11] J.M. Jornet, J.C. Pujol, J.S. Pareta, PHLAME: a physical layer aware MAC protocol for electromagnetic nanonetworks in the terahertz band, Nano Commun. Netw. (Elsevier) J. 3 (1) (2012) 74–81.
[12] S. Mohrehkesh, M.C. Weigle, RIH-MAC: receiver-initiated harvesting-aware mac for nanonetworks, in: Proc. of the ACM International Conference on Nanoscale Computing and Communication, ACM NANOCOM, Atlanta, GA, May 2014.
[13] C. Han, I.F. Akyildiz, Distance-aware multi-carrier (DAMC) modulation in terahertz band communication, in: Proc. IEEE International Conference on Communications, accepted to ICC 2014.
[14] A. Geim, K. Novoselov, The rise of graphene, Nature Mater. 6 (2007) 183–191.
[15] A.N. Pal, A. Ghosh, Ultralow noise field-effect transistor from multilayer graphene, Appl. Phys. Lett. 95 (8) (2009).
[16] HITRAN: high-resolution transmission molecular absorption database, Harvard-Smithsonian Center for Astrophysics, Database, 2014. www.cfa.harvard.edu.
[17] Z. Zhang, L. Piatkowski, H. Bakker, M. Bonn, Ultrafast vibrational energy transfer at the water/air interface revealed by two-dimensional surface vibrational spectroscopy, Nat. Chem. 3 (2011) 888–893.
[18] J. Lindnen, P. Vohringer, M. Pshenichnikov, M. Cringus, D. Wiersma, M. Mostovoy, Vibrational relaxation of pure liquid water, Chem. Phys. Lett. 421 (2006) 329–333.
[19] I. Oppermann, M. Hamalainen, J. Iinatti, UWB Theory and Applications, Wiley, 2004.

Pavel Boronin received his M.Sc. degree in Communication Networks and Switching Systems from Saint Petersburg State University of Telecommunications, Russia, in 2012. He is pursuing his studies at the same university and now is a 2nd year Ph.D. student. Since 2014 Pavel has been studying as an exchange Ph.D. student at Tampere University of Technology, Tampere, Finland. His research interests include physics of terahertz radiation, nanonetworks, adaptive routing algorithms for dynamic and static wireless networks.

Vitaly Petrov received his M.Sc. degree in Information Systems Security from SUAI University, St Petersburg, Russia, in 2011. He is now a graduate M.Sc. student at Tampere University of Technology, Tampere, Finland. Since 2014 Vitaly holds a position of Visiting Scholar at School of Electrical and Computer Engineering, Georgia Institute of Technology, GA, USA. From 2011 till 2014 he has been working as a Researcher at the Department of Electronics and Communications Engineering, Tampere University of Technology. Prior to this, from 2008 till 2011 he served as a Junior Researcher with Information Systems Security Department, SUAI, St Petersburg, Russia, as well as an Engineer in Nokia-SUAI joint lab. From May till October 2012 he was a Strategic Intern with Security Research Team at Nokia Research Centre, Helsinki, Finland. Vitaly is a student member of the IEEE and the ACM. His current research interests include Internet-of-Things, Nanonetworks, Cryptology and Network Security.

Dmitri Moltchanov is a Senior Research Scientist in the Department of Electronics and Communications Engineering, Tampere University of Technology, Finland. He received his M.Sc. and Cand.Sc. degrees from Saint Petersburg State University of Telecommunications, Russia, in 2000 and 2002, respectively, and Ph.D. degree from Tampere University of Technology in 2006. His research interests include performance evaluation and optimization issues of wired and wireless IP networks, Internet traffic dynamics, quality of user experience of real-time applications, and traffic localization P2P networks. Dmitri Moltchanov serves as the TPC member in a number of international conferences. He authored more than 50 publications.

Yevgeni Koucheryavy is a Full Professor and Lab Director at the Department of Electronics and Communications Engineering at the Tampere University of Technology (TUT), Finland. He received his Ph.D. degree (2004) from the TUT. Yevgeni is the author of numerous publications in the field of advanced wired and wireless networking and communications. His current research interests include various aspects in heterogeneous wireless communication networks and systems, the Internet of Things and its standardization, and nanocommunications. Yevgeni is an Associate Technical Editor of IEEE Communications Magazine and Editor of IEEE Communications Surveys and Tutorials. Yevgeni is a Senior IEEE member.

Josep Miquel Jornet received the Engineering Degree in Telecommunication and the Master of Science in Information and Communication Technologies from the Universitat Politècnica de Catalunya, Barcelona, Spain, in 2008. He received the Ph.D. degree in Electrical and Computer Engineering from the Georgia Institute of Technology, Atlanta, GA, in 2013, with a fellowship from "la Caixa" (2009–2010) and Fundación Caja Madrid (2011–2012). He is currently an Assistant Professor with the Department of Electrical Engineering at the University at Buffalo, The State University of New York. From September 2007 to December 2008, he was a visiting researcher at the Massachusetts Institute of Technology, Cambridge, under the MIT Sea Grant program. He was the recipient of the Oscar P. Cleaver Award for outstanding graduate students in the School of Electrical and Computer Engineering, at the Georgia Institute of Technology in 2009. He also received the Broadband Wireless Networking Lab Researcher of the Year Award at the Georgia Institute of Technology in 2010. He is a member of the IEEE and the ACM. His current research interests include electromagnetic nanonetworks, graphene-enabled wireless communication, Terahertz Band communication networks and the Internet of Nano-Things.